ACS OMEGA

http://pubs.acs.org/journal/acsodf

Article

Flat Zigzag Silicene Nanoribbon with Be Bridge

Masae Takahashi*

Cite This: *ACS Omega* 2021, 6, 12099−12104

Read Online

ACCESS | Metrics & More | Article Recommendations | Supporting Information

ABSTRACT: The emergence of flat one- and two-dimensional materials, such as graphene and its nanoribbons, has promoted the rapid advance of the current nanotechnology. Silicene, a silicon analogue of graphene, has the great advantage of its compatibility with the present industrial processes based on silicon nanotechnology. The most significant issue for silicene is instability in the air due to the nonplanar puckered (buckled) structure. Another critical problem is that silicene is usually synthesized by epitaxial growth on a substrate, which strongly affects the π conjugated system of silicene. The fabrication of free-standing silicene with a planar configuration has long been pursued. Here, we report the strategy and design to realize the flat zigzag silicene nanoribbon. We theoretically investigated the stability of various silicene nanoribbons with substituents at the zigzag edges and found that zigzag silicene nanoribbons with beryllium (Be) bridges are very stable in a planar configuration. The obtained zigzag silicene nanoribbon has an indirect negative band gap and is nonmagnetic unlike the magnetic buckled silicene nanoribbons with zigzag edges. The linearly dispersive behavior of the π and π^* bands associated with the out-of-plane $3p_{si}$ and $2p_{Be}$ orbitals is clearly observed, showing the existence of a Dirac point slightly above the Fermi level. We also observed that spin−orbit coupling induces a gap opening at the Dirac point.

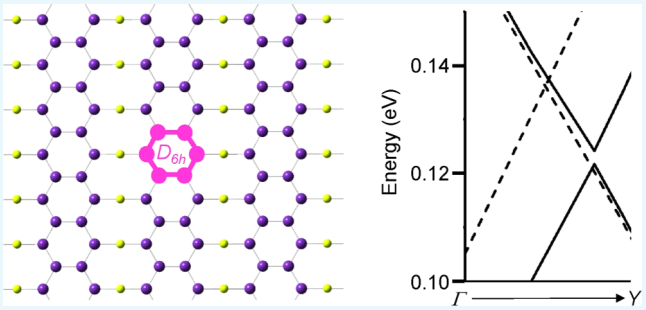

INTRODUCTION

Planar one-dimensional (1D) and two-dimensional (2D) materials, such as graphene and its nanoribbons, have accelerated the rapid development of nanoscience and technology.[1−3] Silicene, a silicon analogue of graphene, is one of the most remarked postgraphene materials. The diverse material properties of the intrinsic and functionalized silicene and its nanoribbons provide a wide degree of freedom in designing more efficient nanodevices.[4] Silicene has the great advantage of its compatibility with the current industrial processes based on silicon nanotechnology. However, silicene involves an inherent problem, namely, instability in the air due to its puckered (buckled) structure.[5−7] Silicene has another critical problem in its material processing. Silicene films are usually fabricated by epitaxial growth on a substrate,[8−18] which inevitably affects the intrinsic π conjugated electron system and, as a result, disturbs the fundamental 2D property.[19−22] So far, intensive efforts have been made to predict/synthesize free-standing silicene with a planar configuration but in almost all cases have resulted in undesired silicene with a buckled honeycomb structure.[23−30] However, attempts to create flat silicene nanoribbons by modifying the edges of the ribbon without disturbing the π conjugated system have been scarcely adopted.

The structural differences between silicene and graphene stem from the differences in the building blocks: flat D_{6h} benzene vs chair-form D_{3d} hexasilabenzene (Figure 1).[31] To obtain flat silicene, it is crucial to design a flat building block with substituents that do not interact with the out-of-plane π orbital. The flat and aromatic six-membered silicon rings have long been pursued in silicon chemistry.[32,33] Based on our previous study on the anionic six-membered silicon rings,[33,34] we recently succeeded in designing a flat building block for flat silicene.[35] Our fundamental strategy is to attach a substituent, which has an sp-hybridized orbital and functions as an electron donor so that it does not interact with the π orbital. Following this concept, a flat hexasilabenzene was achieved using BeH as a substituent at the in-plane edge (Figure 1). Furthermore, our previous study revealed that extended polycyclic molecules containing two to six hexagons were also flat when BeH was attached to the in-plane edge (Figure 1). These honeycomb silicon molecules with BeH at the in-plane edges exhibit the same structure, charge distribution, and molecular orbital characteristics as the corresponding carbon-based molecules. This suggests that further extensions to infinity may provide planar 2D silicene if it is BeH-saturated at the edges. This finding motivated us to design flat silicene nanoribbons as computable silicene materials

Received: February 11, 2021
Accepted: March 29, 2021
Published: April 29, 2021

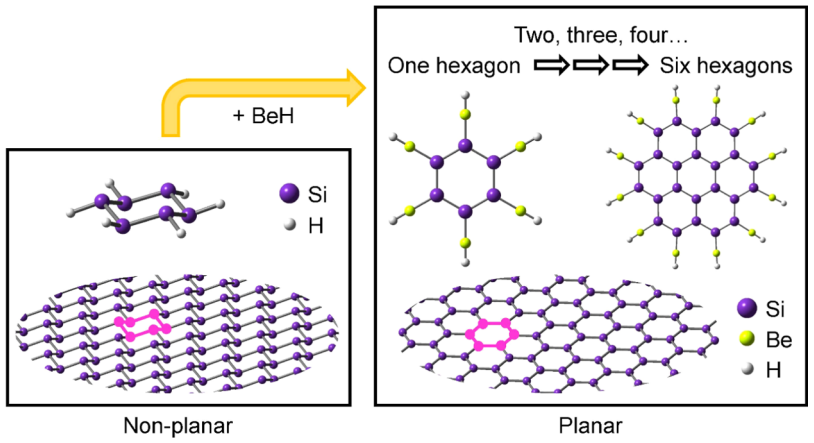

Figure 1. Chair-form hexasilabenzene as a building block of buckled silicene (left); flat BeH-terminated hexasilabenzene and flat BeH-terminated coronene silicon analogue as building blocks of planar silicene (right). The building blocks in the silicene sheet are marked in bright red.

with both periodic boundary conditions and in-plane-edge substituents.

Here, we report a successful design for a free-standing single-layer silicene nanoribbon with a planar configuration using density functional theory (DFT) calculation. The silicene honeycomb structure produces two different edges, an armchair and a zigzag, defined by the orientation of the hexagon with respect to the ribbon. We search for zigzag silicene nanoribbons (ZSiNRs) with a flat configuration among several possible structures with various substituents at the in-plane edges, such as 2-, 4-, and 6-chains with Be/Mg bridges or BeH/MgH terminations. The stability of the flat structure was examined by frequency calculations. In the following, we describe the structural and electronic properties of the obtained flat silicene nanoribbon, a 2-chain with a Be bridge at the zigzag edge. We found that the flat structure in all other nanoribbons examined in this study was not a stable minimum.

RESULTS AND DISCUSSION

Optimized Structure with Flat Configuration. The designed free-standing flat monolayer silicene nanoribbon, a 2-chain with a Be bridge at the zigzag edge (Be-bridged 2-chain ZSiNR, Figure 2a), is composed of silicon hexagons with nearly D_{6h} group symmetry. The Be atom functions as an electron donor and connects to the silicene nanoribbon using sp-hybridized orbitals. The most similar nanoribbon to the Be-bridged 2-chain ZSiNR examined here is the BeH-terminated 2-chain silicene nanoribbon (BeH-terminated 2-chain ZSiNR, Figure 2b). We compare these two different 2-chain silicene nanoribbons. The Be-bridged 2-chain ZSiNR is a 2D crystal because 1D nanoribbons are connected by Be atoms to form a periodic 2D sheet. On the other hand, the BeH-terminated 2-chain ZSiNR is a 1D chain. Therefore, a 2D unit cell with sufficient vacuum was used to calculate the BeH-terminated 2-chain ZSiNR. See the Computational Details section for details. A 2D unit cell of Be-bridged 2-chain ZSiNR contains five atoms, one Be atom and four Si atoms (Figure 2a), while that of BeH-terminated 2-chain ZSiNR contains eight atoms, two BeH groups and four Si atoms (Figure 2b). We have confirmed that the 2-chain ZSiNRs do not show (2×1) reconstruction along the 2-chain direction.

Geometry optimizations for the Be-bridged and BeH-terminated 2-chain ZSiNRs in Figure 2 were performed under planar D_{2h} group symmetry. The optimized planar Be-bridged 2-chain ZSiNR is the minimum without imaginary frequencies, while the planar BeH-terminated 2-chain ZSiNR is a transition state with two imaginary frequencies. The hexagons in both 2-chain nanoribbons have nearly D_{6h} group symmetry: six silicon−silicon bond lengths are almost the same with a difference of less than 1%, and the six bond angles take 120° within an error of less than 2%. This indicates that although the two out-of-plane BeH bending modes in the BeH-terminated 2-chain ZSiNR show imaginary values, the geometric properties of the six-membered silicon ring differ only slightly between the two nanoribbons. In that sense, the 2-chain skeleton of BeH-terminated 2-chain ZSiNR may flatten with BeH bent out of plane. We challenged to obtain the minimum structure of BeH-terminated 2-chain ZSiNR with keeping the 2-chain skeleton flat, but we could not obtain it. All other silicene nanoribbons bearing substituents at the zigzag edges in a flat configuration (Mg-bridged 2-chain ZSiNR, Be-bridged 4- and 6-chain ZSiNRs, BeH-terminated 4-chain ZSiNR) gave imaginary values for out-of-plane ring deformation modes, resulting in a nonplanar buckling configuration at the minimum (for details, see Table S1). The width of the nanoribbon is an interesting parameter for the electronic properties of the ribbon. However, we could not

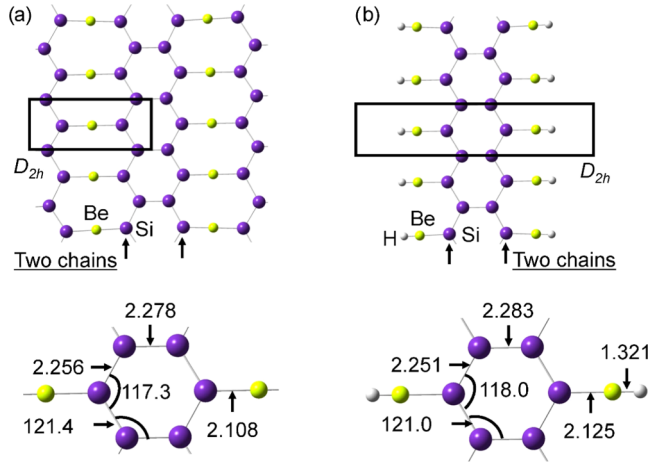

Figure 2. (a) Be-bridged 2-chain nanoribbon (Be-bridged 2-chain ZSiNR) and (b) BeH-terminated 2-chain nanoribbon (BeH-terminated 2-chain ZSiNR). The geometric parameters of the optimized flat structure are given in Å for bond length and degree for bond angle. The unit cells of a 2D crystal are shown as rectangles with group symmetry.

https://doi.org/10.1021/acsomega.1c00794
ACS Omega 2021, 6, 12099−12104

obtain nanoribbons with widened widths such as 4- and 6-chains as a stable minimum in the planar configuration. As a result, we were unable to investigate the effect of ribbon width.

Table 1 compares the silicon−silicon bond lengths among Be-bridged 2-chain ZSiNR, hexasilabenzene, BeH-terminated hexasilabenzene, and silicene. The periodic calculations of BeH-terminated hexasilabenzene and planar hexasilabenzene with sufficient vacuum space between the molecules reproduce the previous gas-phase calculations.[35] That is, in both periodic and gas-phase calculations, planar BeH-terminated hexasilabenzene is the minimum, while planar hexasilabenzene is the transition state. In addition, when compared between periodic and gas-phase calculations, the Si−Si bond distances are almost equal within an error of 0.001 Å, and the lowest frequencies match within an error of 1.5 cm^{-1}. The Si−Si bond length of hexasilabenzene with a flat configuration is slightly shorter (2.216 Å) than that of the minimum planar molecule, BeH-terminated hexasilabenzene (2.251 Å). The zigzag chain part of the Be-bridged 2-chain ZSiNR provides a Si−Si bond length of 2.256 Å, similar to that of planar silicene (2.254 Å), while the Si−Si bond connecting the two chains in the Be-bridged 2-chain ZSiNR has about the same bond length (2.278 Å) as nonplanar silicene (2.279 Å). The lattice constants and Si−Si bond lengths obtained in this study for buckled (nonplanar) silicene are the same as those in the previous calculations[36] ($a = b = 3.87$ Å, $\alpha = \beta = 90°$, $\gamma = 120°$, r(Si−Si) = 2.28 Å). In both our current and previously reported calculations, planar silicene is not a minimum state, but a transition state with an imaginary frequency, indicating that it is inherently unstable. The imaginary frequency of planar silicene is associated with the out-of-plane optical mode. This out-of-plane vibration enhances the atomic buckling, leading to a nonplanar buckling configuration.

Table 1. Silicon−Silicon Bond Length (r(Si−Si)) and the Lowest Frequency (ν_1) of Optimized Molecules and Sheets

molecule or sheet	structure	SP[a]	r(Si−Si) (Å)[b]	ν_1 (cm^{-1})
Be-bridged 2-chain ZSiNR	planar	MIN	2.256, 2.278	15.4
hexasilabenzene	planar	TS	2.216	
BeH-terminated hexasilabenzene	planar	MIN	2.251 (2.252)	46.1 (47.6)
silicene	planar	TS	2.254	
silicene	nonplanar	MIN	2.279	175.3

[a]SP: stationary point, TS: transition state, MIN: minimum. [b]The result [ref 35] of gas-phase calculation is in parentheses.

Band Structure. The planar Be-bridged 2-chain ZSiNR has an indirect negative band gap. That is, the conduction-band minimum lies lower than the valence-band maximum (Figure 3a). We performed spin-polarized total-energy and electronic-structure calculations of the planar Be-bridged 2-chain ZSiNR and compared the results with those of the spin-unpolarized. We find that there is no essential difference in the gross band structure between spin-polarized and spin-unpolarized calculations. This shows that the flat Be-bridged 2-chain ZSiNR is nonmagnetic, in contrast to the free-standing buckled ZSiNR being magnetic.[37,38] The linear dispersive behavior of the bands and their crossing are clearly observed at the valence-band maximum midway between the Γ and Y points in the rectangular Brillouin zone of the Be-bridged 2-chain ZSiNR (Figure 3a), indicating the existence of a Dirac point near the Y point. A similar band-crossing of the linearly dispersive bands indicating the Dirac point is also observed at the K point in the hexagonal Brillouin zone of buckled silicene (Figure 3b).[37]

The linearly dispersive bands 1 and 2 of the Be-bridged 2-chain ZSiNR are ascribed to the π and π^* bands associated with the out-of-plane $3p_{si}$ and $2p_{Be}$ orbitals (Figure 4a), while in buckled silicene the buckling of Si atoms causes sp^2−sp^3 hybridizations. As shown in the orbital-projected DOS of the Be-bridged 2-chain ZSiNR in Figure 3a, the contribution of the p_{si} and p_{Be} orbitals is certainly dominant near the Fermi level and the contribution of the s_{si} and s_{Be} orbitals is negligible. It is remarked that the band-crossing point (Dirac point) near the Y point in the Be-bridged 2-chain ZSiNR is located slightly above the Fermi level (Figure 3a). At the S point in the Be-bridged 2-chain ZSiNR, the conduction band is associated with the in-plane $2p_{//Be}$ orbital along the chain direction shown by the band 3 orbital in Figure 4a and is inserted between the π and π^* bands. The minimum of the $2p_{//Be}$ band is located below the Fermi level. This indicates that the Be-bridged 2-chain ZSiNR is semimetal, with a hole pocket near the Y point and an electron pocket at the S point (Figure 5).

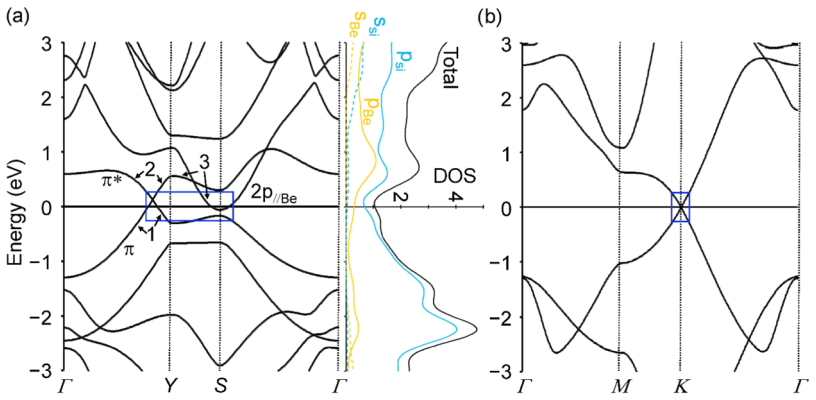

Figure 3. Electronic band structures with spin−orbit coupling along high-symmetry lines of the 2D Brillouin zone of (a) Be-bridged 2-chain ZSiNR and (b) buckled silicene. The reference zero energy corresponds to the Fermi level. The Brillouin zone path (Γ → Y → S → Γ) is shown in Figure 5. The magnifications around the band gaps (marked by the blue rectangles) are shown in Figure 6. The orbitals of bands 1 and 2 between the Γ and Y points and band 3 between the Y and S points are shown in Figure 4. The orbital-projected density of states (DOS) for the Be-bridged 2-chain ZSiNR is given in the right panel of (a).

https://doi.org/10.1021/acsomega.1c00794
ACS Omega 2021, 6, 12099−12104

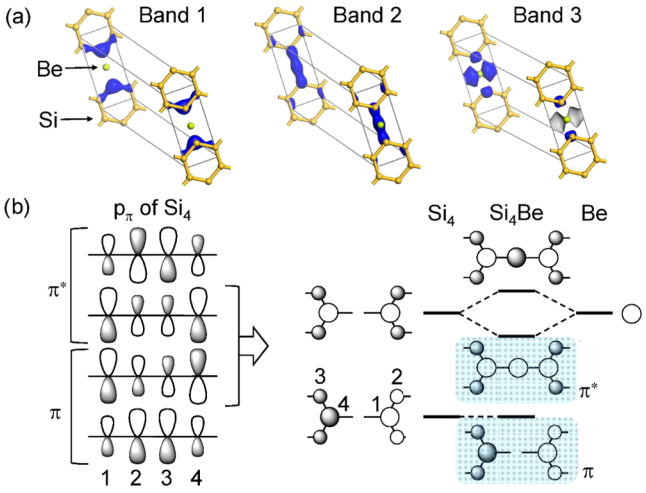

Figure 4. (a) Isosurfaces of the orbitals in the unit cells that constitute bands 1, 2, and 3 in Figure 3a. The outside of the isosurface is bright blue, and the inside is gray. (b) Schematic π orbitals of Si_4 from the side of the molecular plane (left). Energy diagram of the interaction between the two π orbitals of Si_4 and the $2p_{Be}$ orbital (right). The schematic orbitals at each energy level are depicted from the top of the molecular plane. The out-of-plane p_π orbitals of the four Si atoms are numbered 1−4. The π and π^* orbitals that constitute bands 1 and 2 are marked with blue boxes, respectively.

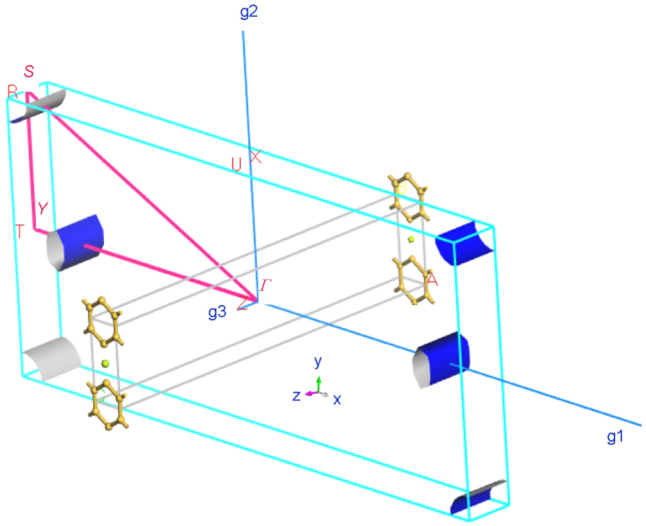

Figure 5. Brillouin zone and Fermi surface (indicated by the blue sheet) of the Be-bridged 2-chain ZSiNR. Cartesian coordinates in real space and lattice vectors in reciprocal space are represented by (x, y, z) and (g1, g2, g3), respectively.

Figure 4b shows an orbital interaction diagram that illustrates the orbitals of band 1 and band 2. As shown in the left panel of Figure 4b, the out-of-plane 3p orbitals of the four silicon atoms in the unit cell form four π orbitals, two π and two π^*. The lower π^*orbital of Si_4 interacts with the out-of-plane $2p_{Be}$ orbital, giving band 2 in Figure 4a. On the other hand, the higher π orbital of Si_4 does not interact with the out-of-plane $2p_{Be}$ orbital due to symmetry, giving band 1 in Figure 4a.

We observed that when the spin−orbit coupling is included in the calculations of the Be-bridged 2-chain ZSiNR, the energy gap opens at the Dirac point and at the same time the gap at the S point is enlarged. Figure 6 shows the magnification around the band gaps marked by the blue rectangle in Figure 3. The solid and dashed lines show the band structures with and without the spin−orbit coupling, respectively. The magnitude of the gap induced at the Dirac point is 2.4 meV, which is comparable to the gap size in buckled silicene.[39] We also observed that the Dirac point moves toward the *Y* point, including the spin−orbit coupling (Figure 6a), in contrast to the buckled silicene where the Dirac point is pinned at the *K* point (Figure 6b). On the other hand, it can be seen that the spin−orbit coupling causes an enhancement in the band gap at the *S* point from 102 to 109 meV (Figure 6a). The overlap between the conduction and valence bands of the Be-bridged 2-chain ZSiNR is estimated to be 182 meV including the spin−orbit coupling.

The theoretically designed Be-bridged 2-chain ZSiNR is air-stable due to its flatness and has the potential to be applied to high-speed 2D switching devices due to the existence of sufficient band gap at the Dirac point. A Be-bridged 2-chain ZSiNR could be synthesized by placing Be atoms on a 1D grating dip of a silicene nanoribbon[27] using a recently developed atomic-scale manipulation.[40]

CONCLUSIONS

We have reported strategies and designs for fabricating flat silicene nanoribbons using solid-state DFT calculations. The obtained Be-bridged 2-chain ZSiNR shows a stable minimum in a flat configuration, with each hexagon in the ribbon maintaining D_{6h} group symmetry. We found that the Be-bridged 2-chain ZSiNR is nonmagnetic, in contrast to the magnetic buckled ZSiNR. The Be-bridged 2-chain ZSiNR is a semimetal with a hole pocket near the *Y* point in the Brillouin zone and an electron pocket at the *S* point. The crossing of two linearly dispersive bands showing the Dirac-fermion nature is clearly observed slightly above the Fermi level near the *Y* point. Spin−orbit coupling induces the opening of a small energy gap at the Dirac point. The present proposal to create a stable, free-standing, flat silicene nanoribbon would pave the way for the rapid development of silicene nanotechnology.

COMPUTATIONAL DETAILS

We performed structural and electronic calculations in the DFT framework, as implemented in CASTEP code (ver. 2018).[41] The total-energy calculation was based on the plane-wave DFT method within a generalized gradient approximation. The Perdew−Burke−Ernzerhof exchange-correlation functional[42,43] was used as implemented in the CASTEP code. Norm-conserving pseudopotentials were used to describe electron−ion interactions. A fully relativistic norm-conserving pseudopotential was used to examine the effects of spin−orbit coupling. We described the geometric structure under the periodic boundary conditions, adopting rectangular cells for the ribbon and hexagonal cells for the molecules and buckled silicene. To avoid spurious interactions between the periodically repeated replicas, we set vacuum regions of 30−45 and 78 Å (30 Å for hexasilabenzene) perpendicular and parallel to the molecular, ribbon, and sheet planes, respectively. The valence electron wavefunction was expanded in terms of the plane-wave basis set to a 1200 eV kinetic energy cutoff. The electronic minimization was converged to less than 10^{-10} eV/atom using a conjugate gradient scheme (the force on each atom was reduced to below 10^{-5} eV/Å). Brillouin zone integration was performed with the Monkhorst−Pack method using *k*-point mesh with intervals less than 0.01 $Å^{-1}$. The total energy of the system converged to better than 0.1 meV/atom for *k*-point sampling.

https://doi.org/10.1021/acsomega.1c00794
ACS Omega 2021, 6, 12099−12104

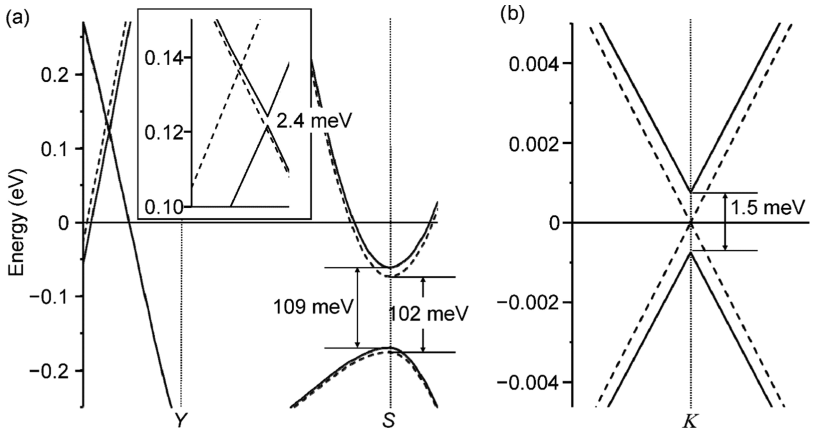

Figure 6. Magnification of the band structure of the band gap region marked by the blue rectangles in Figure 3 of (a) Be-bridged 2-chain ZSiNR and (b) buckled silicene. The solid and dashed lines are the results with and without spin−orbit coupling, respectively. The inset in (a) is a further magnification around the Dirac point.

The geometries were fully optimized for both the cell parameters and atomic coordinates under the constraints of group symmetry of D_{6h} for the molecules and D_{2h} for the ribbon. The vibrational frequencies of the normal modes were calculated at the Γ-point within the harmonic approximation by linear response theory (or density functional perturbation theory),[44] which provides an analytical strategy for computing the second derivative of the total energy with respect to a given perturbation. We confirmed that there is no imaginary mode for minimum structure and that there are three phonon modes with zero frequency. Three phonon modes with zero frequency are necessary, as the total energy should be invariant under the translation of the entire crystal.

■ ASSOCIATED CONTENT

Supporting Information

The Supporting Information is available free of charge at https://pubs.acs.org/doi/10.1021/acsomega.1c00794.

Results of other ZSiNRs (Table S1) (PDF)

■ AUTHOR INFORMATION

Corresponding Author

Masae Takahashi − *Graduate School of Agricultural Science, Tohoku University, Sendai 980-8572, Japan;* orcid.org/0000-0001-7717-6512; Email: masae@fris.tohoku.ac.jp

Complete contact information is available at: https://pubs.acs.org/10.1021/acsomega.1c00794

Notes

The author declares no competing financial interest.

■ ACKNOWLEDGMENTS

The author acknowledges the Center for Computational Materials Science of IMR, Tohoku University. This work was supported by the Collaborative Research Program of Institute for Chemical Research, Kyoto University (Grant Nos. 2018-107, 2019-118, and 2020-128).

■ ABBREVIATIONS

1D, one-dimensional; 2D, two-dimensional; DFT, density functional theory; ZSiNR, zigzag silicene nanoribbon; DOS, density of states

■ REFERENCES

(1) Fiori, G.; Bonaccorso, F.; Iannaccone, G.; Palacios, T.; Neumaier, D.; Seabaugh, A.; Banerjee, S. K.; Colombo, L. Electronics based on two-dimensional materials. *Nat. Nanotechnol.* **2014**, *9*, 768−779.

(2) Magda, G. Z.; Jin, X.; Hagymási, I.; Vancsó, P.; Osváth, Z.; Nemes-Incze, P.; Hwang, C.; Biró, L. P.; Tapasztó, L. Room-temperature magnetic order on zigzag edges of narrow graphene nanoribbons. *Nature* **2014**, *514*, 608−611.

(3) Heerema, S. J.; Dekker, C. Graphene nanodevices for DNA sequencing. *Nat. Nanotechnol.* **2016**, *11*, 127−136.

(4) Molle, A.; Goldberger, J.; Houssa, M.; Xu, Y.; Zhang, S.-C.; Akinwande, D. Buckled two-dimensional Xene sheets. *Nat. Mater.* **2017**, *16*, 163−169.

(5) Tao, L.; Cinquanta, E.; Chiappe, D.; Grazianetti, C.; Fanciulli, M.; Dubey, M.; Molle, A.; Akinwande, D. Silicene field-effect transistors operating at room temperature. *Nat. Nanotechnol.* **2015**, *10*, 227−231.

(6) Peplow, M. Silicene makes its transistor debut. *Nature* **2015**, *518*, 17−18.

(7) Brumfiel, G. Sticky problem snares wonder material. *Nature* **2013**, *495*, 152−153.

(8) Vogt, P.; De Padova, P.; Quaresima, C.; Avila, J.; Frantzeskakis, E.; Asensio, M. C.; Resta, A.; Ealet, B.; Lay, G. L. Silicene: compelling experimental evidence for graphenelike two-dimensional silicon. *Phys. Rev. Lett.* **2012**, *108*, No. 155501.

(9) Feng, B.; Ding, Z.; Meng, S.; Yao, Y.; He, X.; Cheng, P.; Chen, L.; Wu, K. Evidence of silicene in honeycomb structures of silicon on Ag(111). *Nano Lett.* **2012**, *12*, 3507−3511.

(10) Gao, J.; Zhao, J. Initial geometries, interaction mechanism and high stability of silicene on Ag(111) surface. *Sci. Rep.* **2012**, *2*, No. 861.

(11) Kaltsas, D.; Tsetseris, L.; Dimoulas, A. Structural evolution of single-layer films during deposition of silicon on silver: a first-principles study. *J. Phys.: Condens. Matter* **2012**, *24*, No. 442001.

(12) Tsoutsou, D.; Xenogiannopoulou, E.; Golias, E.; Tsipas, P.; Dimoulas, A. Evidence for hybrid surface metallic band in (4 × 4) silicene on Ag(111). *Appl. Phys. Lett.* **2013**, *103*, No. 231604.

(13) Moras, P.; Mentes, T. O.; Sheverdyaeva, P. M.; Locatelli, A.; Carbone, C. Coexistence of multiple silicene phases in silicon grown on Ag(111). *J. Phys.: Condens. Matter* **2014**, *26*, No. 185001.

(14) Feng, Y.; Liu, D.; Feng, B.; Liu, X.; Zhao, L.; Xie, Z.; Liu, Y.; Liang, A.; Hu, C.; Hu, Y.; He, S.; Liu, G.; Zhang, J.; Chen, C.; Xu, Z.; Chen, L.; Wu, K.; Liu, Y.-T.; Lin, H.; Huang, Z.-Q.; et al. Direct evidence of interaction-induced Dirac cones in a monolayer silicene/Ag(111) system. *Proc. Natl. Acad. Sci. U.S.A.* **2016**, *113*, 14656−14661.

(15) Du, Y.; Zhuang, J.; Wang, J.; Li, Z.; Liu, H.; Zhao, J.; Xu, X.; Feng, H.; Chen, L.; Wu, K.; Wang, X.; Dou, S. X. Quasi-freestanding epitaxial silicene on Ag(111) by oxygen intercalation. *Sci. Adv.* **2016**, *2*, No. e1600067.

(16) Fleurence, A.; Friedlein, R.; Ozaki, T.; Kawai, H.; Wang, Y.; Yamada-Takamura, Y. Experimental evidence for epitaxial silicene on diboride thin films. *Phys. Rev. Lett.* **2012**, *108*, No. 245501.
(17) Meng, L.; Wang, Y.; Zhang, L.; Du, S.; Wu, R.; Li, L.; Zhang, Y.; Li, G.; Zhou, H.; Hofer, W. A.; Gao, H.-J. Buckled silicene formation on Ir(111). *Nano Lett.* **2013**, *13*, 685−690.
(18) Chiappe, D.; Scalise, E.; Cinquanta, E.; Grazianetti, C.; Broek, B.; Fanciulli, M.; Houssa, M.; Molle, A. Two-dimensional Si nanosheets with local hexagonal structure on a MoS_2 surface. *Adv. Mater.* **2014**, *26*, 2096−2101.
(19) Guo, Z.-X.; Furuya, S.; Iwata, J.-I.; Oshiyama, A. Absence and presence of Dirac electrons in silicene on substrates. *Phys. Rev. B* **2013**, *87*, No. 235435.
(20) Wang, Y.-P.; Cheng, H.-P. Absence of a Dirac cone in silicene on Ag(111): first-principles density functional calculations with a modified effective band structure technique. *Phys. Rev. B* **2013**, *87*, No. 245430.
(21) Cahangirov, S.; Audiffred, M.; Tang, P.; Iacomino, A.; Duan, W.; Merino, G.; Rubio, A. Electronic structure of silicene on Ag(111): strong hybridization effects. *Phys. Rev. B* **2013**, *88*, No. 035432.
(22) Mahatha, S. K.; Moras, P.; Bellini, V.; Sheverdyaeva, P. M.; Struzzi, C.; Petaccia, L.; Carbone, C. Silicene on Ag(111): a honeycomb lattice without Dirac bands. *Phys. Rev. B* **2014**, *89*, No. 201416(R).
(23) Guzmán-Verri, G. G.; Lew Yan Voon, L. C. Electronic structure of silicon-based nanostructures. *Phys. Rev. B* **2007**, *76*, No. 075131.
(24) Lew Yan Voon, L. C.; Zhu, J.; Schwingenschlögl, U. Silicene: recent theoretical advances. *Appl. Phys. Rev.* **2016**, *3*, No. 040802.
(25) Zhao, J.; Liu, H.; Yu, Z.; Quhe, R.; Zhou, S.; Wang, Y.; Liu, C. C.; Zhong, H.; Han, N.; Lu, J.; Yao, Y.; Wu, K. Rise of silicene: a competitive 2D material. *Prog. Mater. Sci.* **2016**, *83*, 24−151.
(26) Takeda, K.; Shiraishi, K. Theoretical possibility of stage corrugation in Si and Ge analogs of graphite. *Phys. Rev. B* **1994**, *50*, No. 14916.
(27) De Padova, P.; Quaresima, C.; Ottaviani, C.; Sheverdyaeve, P. M.; Moras, P.; Carbone, C.; Topwal, D.; Olivieri, B.; Kara, A.; Oughaddou, H.; Aufray, B.; Lay, G. L. Evidence of graphene-like electronic signature in silicene nanoribbons. *Appl. Phys. Lett.* **2010**, *96*, No. 261905.
(28) De Padova, P.; Quaresima, C.; Perfetti, P.; Olivieri, B.; Leandri, C.; Aufray, B.; Vizzini, S.; Lay, G. L. Growth of straight, atomically perfect, highly metallic silicon nanowires with chiral asymmetry. *Nano Lett.* **2008**, *8*, 271−275.
(29) De Padova, P.; Perfetti, P.; Olivieri, B.; Quaresima, C.; Ottaviani, C.; Lay, G. L. 1D graphene-like silicon systems: silicene nano-ribbons. *J. Phys.: Condens. Matter* **2012**, *24*, No. 223001.
(30) Colonna, S.; Serrano, G.; Gori, P.; Cricenti, A.; Ronci, F. Systematic STM and LEED investigation of the Si/Ag(110) surface. *J. Phys.: Condens. Matter* **2013**, *25*, No. 315301.
(31) Nagase, S.; Teramae, H.; Kudo, T. Hexasilabenzene (Si_6H_6). Is the benzene-like D_{6h} structure stable? *J. Chem. Phys.* **1987**, *86*, 4513−4517.
(32) Jose, D.; Datta, A. Structures and chemical properties of silicene: unlike graphene. *Acc. Chem. Res.* **2014**, *47*, 593−602.
(33) Takahashi, M. Polyanionic hexagons: X_6^{n-} (X = Si, Ge). *Symmetry* **2010**, *2*, 1745−1762.
(34) Takahashi, M.; Kawazoe, Y. Theoretical study on planar anionic polysilicon chains and cyclic Si_6 anions with D_{6h} symmetry. *Organometallics* **2005**, *24*, 2433−2440.
(35) Takahashi, M. Flat building blocks for flat silicene. *Sci. Rep.* **2017**, *7*, No. 10855.
(36) Houssa, M.; Dimoulas, A.; Molle, A. Silicene: a review of recent experimental and theoretical investigations. *J. Phys.: Condens. Matter* **2015**, *27*, No. 253002.
(37) Cahangirov, S.; Topsakal, M.; Aktürk, E.; Şahin, H.; Ciraci, S. Two- and one-dimensional honeycomb structures of silicon and germanium. *Phys. Rev. Lett.* **2009**, *102*, No. 236804.
(38) Ding, Y.; Wang, Y. Electronic structures of reconstructed zigzag silicene nanoribbons. *Appl. Phys. Lett.* **2014**, *104*, No. 083111.
(39) Grazianetti, C.; Cinquanta, E.; Molle, A. Two-dimensional silicon: the advent of silicene. *2D Mater.* **2016**, *3*, No. 012001.
(40) Ko, W.; Ma, C.; Nguyen, G. D.; Kolmer, M.; Li, A.-P. Atomic-scale manipulation and in situ characterization with scanning tunneling microscopy. *Adv. Funct. Mater.* **2019**, *29*, No. 1903770.
(41) Clark, S. J.; Segall, M. D.; Pickard, C. J.; Hasnip, P. J.; Probert, M. I. J.; Refson, K.; Payne, M. C. First principles methods using CASTEP. *Z. Kristallogr.* **2005**, *220*, 567−570.
(42) Perdew, J. P.; Burke, K.; Ernzerhof, M. Generalized gradient approximation made simple. *Phys. Rev. Lett.* **1996**, *77*, No. 3865.
(43) Perdew, J. P.; Burke, K.; Ernzerhof, M. ERRATA: generalized gradient approximation made simple. [Phys. Rev. Lett. 77, 3865 (1996)]. *Phys. Rev. Lett.* **1997**, *78*, No. 1396.
(44) Baroni, S.; Gironcoli, S.; Corso, A. D.; Giannozzi, P. Phonons and related crystal properties from density-functional perturbation theory. *Rev. Mod. Phys.* **2001**, *73*, No. 515.

https://doi.org/10.1021/acsomega.1c00794
ACS Omega 2021, 6, 12099−12104